



SAKARYA ÜNİVERSİTESİ

FEN BİLİMLERİ ENSTİTÜSÜ DERGİSİ

Sakarya University Journal of Science
SAUJS

e-ISSN: 2147-835X | Founded: 1997 | Period: Bimonthly | Publisher: Sakarya University
<http://www.saujs.sakarya.edu.tr/en/>

Title: Extended Back-EMF Based Industrial Sensorless Drive System for PMSMs

Authors: Burak GÖRDÜK, Murat YILMAZ

Received: 2021-01-25 01:29:47

Accepted: 2021-07-13 14:12:56

Article Type: Research Article

Volume: 25

Issue: 4

Month: August

Year: 2021

Pages: 1049-1060

How to cite

Burak GÖRDÜK, Murat YILMAZ; (2021), Extended Back-EMF Based Industrial Sensorless Drive System for PMSMs. Sakarya University Journal of Science, 25(4), 1049-1060, DOI: <https://doi.org/10.16984/saufenbilder.867649>

Access link

<http://www.saujs.sakarya.edu.tr/en/pub/issue/64755/867649>

New submission to SAUJS

<http://dergipark.org.tr/en/journal/1115/submission/step/manuscript/new>

Extended Back-EMF Based Industrial Sensorless Drive System for PMSMs

Burak GÖRDÜK*¹, Murat YILMAZ¹

Abstract

Field Oriented Control (FOC) of Permanent Magnet Synchronous Motors (PMSM) is utilized in many industrial applications due to its high performance. Semiconductor manufacturers provide specialized solutions and tools for this technique. However, such solutions are protected with closed source codes. This reduces the flexibility and the performance of such systems. This paper presents the conducted studies of controller and embedded software design for FOC of a PMSM using extended back-Electromotive Force (EMF) observer. Observer is derived from motor analytical model. Accurate position and speed estimations are observed using the simulations. An inverter board is obtained from market and a controller board with microcontroller is designed. Extended back-EMF observer model is implemented in embedded software. The developed drive system is fully capable to replace the existing closed source solutions with the benefits of having a robust and flexible structure that can be fine-tuned according to the application. Performance in nominal speed range with no-load and full-load along with transient loading is tested with a 3000 rpm industrial fan motor. The developed drive system is capable to operate down to 200 rpm and maintain stability under load disturbances, compensating the 10% speed error during nominal load transitions in one second.

Keywords: Permanent magnet synchronous motor, field oriented control, sensorless, back-electromotive force, observer

1. INTRODUCTION

Electric motor driven systems became the backbone of the way of life we know today. Countless applications count on electric machines. It is estimated that half of the power generated globally is consumed by electric motors [1]. In many high-tech applications such as defense industry, aerospace, aviation and electric vehicles, nature of the application and sector requires using of the best performing technologies and components. For some other industries such

as white and brown goods and industrial applications, domestic and global regulations provide requirements of using efficient and environment-friendly technologies [2]. This high-level specification on drive systems design is then followed as replacing old fashioned induction and DC motors with efficient motors.

Permanent Magnet Synchronous Motors (PMSM) count on permanent magnets placed on rotor for field flux generation. These motors should have a rotating stator field synchronous to rotor field. Thus, using of a driver is necessary with such

* Corresponding author: burakgorduk@gmail.com

¹ Istanbul Technical University, Department of Electrical Engineering, Istanbul, Turkey.

E-Mail: myilmaz@itu.edu.tr

ORCID: <https://orcid.org/0000-0002-2333-0649>; <https://orcid.org/0000-0003-1584-1788>.

motors. Objective of the driver is to apply three-phase voltages to stator, which generates a field vector that is perpendicular to rotor field vector in order to generate maximum torque and drive the motor in an efficient way. Nature of these drive systems require accurate rotor position information. This information can be obtained by utilizing sophisticated position sensors like Hall-effect sensors, encoders and resolvers. Although these sensors provide position information that is crucial for vector control, an undeniable burden comes with utilization of position sensors. Increased size, complexity and cost of motor production combined with the increased maintenance frequency due to position sensors, push designers and researches on developing methods of rotor position estimation without position sensors. In many products, especially home appliances, sensorless vector control is much appreciated and used.

Sensorless vector control made its way to literature in late 1980's especially emerging from T. Ohtani's studies [3]. In his proposed method, a rotor flux estimator with a lag circuit imposing the induced voltage of motor and command of the rotor flux, thus enabling calculation of rotor flux even at standstill. He also states his method as being less dependent to motor parameters than conventional vector control strategies. Systems utilizing Model Reference Adaptive Control (MRAC) were also developed for speed estimation from measured voltage and current values [4 - 6]. Estimated speed is then used as feedback of the vector control system. MRAC based systems contain pure integrators that are affected from resistance change due to thermal variations. Change of resistance due to temperature can be compensated using MRAC [7]. F.Z J. Holtz and J. Quan also used pure integrator for stator flux estimation [8]. With the help of a nonlinear inverter model, their model self-adjusted voltage distortions while drift components were compensated by offset identification. This method shown high dynamic performance even at very low speeds but unable to estimate speed at near standstill points.

An additional emphasis should be laid on position estimation schemes used in sensorless vector

control. Various types of observers, state filters and controllers are proposed as position estimators. Luenberger type observers can be used in such schemes, providing observation of system state vector while identifying the system parameters [9]. Extended Luenberger observer can be utilized for a nonlinear dynamical system and it observes rotor flux while identifying rotor time constant simultaneously [10]. Luenberger observers are also utilized for back-electromotive force (EMF) and flux linkage estimation [11, 12]. Studies with rotor position estimation based on flux linkages are also presented [13, 14]. Flux linkages are obtained by the use of integrators. The problem with these schemes is that integration drift and offset may eventually degrade the estimator performance [15]. Using of an Extended Kalman Filter (EKF) is proposed to eliminate the errors caused by these drifts and offsets [16]. EKF is utilized for sensorless control of PMSM [17]. Though EKF performs well under nominal conditions, this method has issues at startup due to divergence of the EKF estimator. Moreover, computational complexity of EKF is also a burden to processing power in the digital controller side. Use of Sliding Mode Observers (SMO) is proposed for electric drives due to the benefits of order reducing, disturbance rejection and parameter insensitivity [18 - 20]. Robustness of the controller is supported by the use of adaptive methods in a Brushless DC Motor (BLDC) driver, which filled the gaps of unfavorable aspects of EKF [21]. SMO is further investigated in drive systems of PMSM for back-EMF estimation [22].

This paper presents the studies conducted for designing a sensorless vector control system for PMSMs. The study concentrated on the design of a controller board and requisite software for FOC of a PMSM. Sensorless position estimation is based on a Luenberger type extended back-EMF observer. Theory of the observer is explained in detail with motor mathematical model. Operation of the observer is verified by simulations. Position and speed estimation is found accurate and dynamic. Drive system is then verified by laboratory experiments. A controller board is designed in order to be used with an inverter board. Necessary embedded software is

developed for a 32-bit microcontroller on the controller board. Drive system is operated without position sensors for the whole working range. Loading conditions and transient response of the system is tested. Drive system responded fast and maintained stable operation under load disturbances. At the end of the study, a reusable and reconfigurable drive system is developed. This system can replace the industrial solutions with closed source codes. This provides flexibility and fine-tuning based on the application.

This paper presents the general background and the motivation of the study in Chapter 1. Theory of operation and modeling of PMSM is given in Chapter 2. Chapter 3 provides information on the position and speed estimation using extended back-EMF observer. Simulations of the position estimation scheme are presented in Chapter 4. Chapter 5 explains the hardware and embedded software design of the system. Experimental results are given in detail in Chapter 6.

2. FIELD ORIENTED CONTROL OF PMSM

2.1. Mathematical Model of PMSM

It is useful to analyze electric motors using their mathematical expressions. This is achieved by converting the electrical equivalent model of the motors into mathematical models. Three-phase PMSM can be mathematically modeled with the phase voltages expressed as in equation 1.

$$\begin{bmatrix} u_a \\ u_b \\ u_c \end{bmatrix} = R_s \cdot \begin{bmatrix} i_a \\ i_b \\ i_c \end{bmatrix} + \rho \begin{bmatrix} L_a & M_{ab} & M_{ac} \\ M_{ab} & L_b & M_{bc} \\ M_{ac} & M_{bc} & L_c \end{bmatrix} \cdot \begin{bmatrix} i_a \\ i_b \\ i_c \end{bmatrix} + \begin{bmatrix} L_a & M_{ab} & M_{ac} \\ M_{ab} & L_b & M_{bc} \\ M_{ac} & M_{bc} & L_c \end{bmatrix} \cdot \rho \begin{bmatrix} i_a \\ i_b \\ i_c \end{bmatrix} + \begin{bmatrix} e_a \\ e_b \\ e_c \end{bmatrix} \quad (1)$$

where, u_a , u_b and u_c are the three-phase voltages, i_a , i_b and i_c are the three-phase currents, R_s is the phase resistance, ρ is the derivative operator, M_{ab} , M_{ac} and M_{bc} are the mutual inductances, L_a , L_b and L_c are the self-inductances, e_a , e_b and e_c are the three phase induced back-EMF voltages that are given in equation 2.

$$\begin{bmatrix} e_a \\ e_b \\ e_c \end{bmatrix} = \omega_e \cdot \Psi_{PM} \cdot \rho \begin{bmatrix} \cos(\theta_e) \\ \cos(\theta_e - 2\pi/3) \\ \cos(\theta_e + 2\pi/3) \end{bmatrix} \quad (2)$$

where, ω_e is the electrical speed of rotor, Ψ_{PM} is the flux linkage of the permanent magnets and θ_e is the rotor electrical position. Maximum torque is generated when stator field vector is perpendicular to flux linkage of permanent magnets. Considering only the fundamental signals, generated torque on the machine air gap is expressed in equation 3.

$$T_e = \frac{i_a \cdot e_a}{\omega_e} + \frac{i_b \cdot e_b}{\omega_e} + \frac{i_c \cdot e_c}{\omega_e} \quad (3)$$

where, T_e is the electrical torque generated in air gap. In this expression, phase back-EMF waveforms are generated according to winding distributions on the stator and the generated flux according to magnetization technique used on permanent magnets. Stator windings of a PMSM are usually distributed in such a way to generate sinusoidal back-EMF voltage. For the torque equation, phase currents and back-EMFs should match. Otherwise, torque ripple can be generated on the output that is not desired. In order to maintain a smooth torque output, phase currents has to be generated sinusoidal. Electrical torque in the air gap can be coupled with mechanical characteristics of the machine in order to compute operating point of the machine as given in equation 4.

$$J_m \cdot \frac{d}{dt} \omega_e = T_e - T_L - B_m \cdot \omega_e \quad (4)$$

where, J_m is mechanical inertia, B_m is viscous friction coefficient, T_L is mechanical load applied on the shaft.

2.2. PMSM in Rotating Reference Frame

Stator voltage equation of the motor is obtained using Clarke and Park transformations on the fundamental model with the assumption of angle input of the Park transformation is rotor electrical angle. This way, obtained d - q axis variables are

defined in a synchronous rotating reference frame. Stator voltage equations are expressed as given in equation 5.

$$\begin{bmatrix} u_d \\ u_q \end{bmatrix} = \begin{bmatrix} R_s & -\omega_e L_q \\ \omega_e L_d & R_s \end{bmatrix} \cdot \begin{bmatrix} i_d \\ i_q \end{bmatrix} + \begin{bmatrix} L_d & 0 \\ 0 & L_q \end{bmatrix} \cdot \rho \cdot \begin{bmatrix} i_d \\ i_q \end{bmatrix} + \omega_e \cdot \psi_{PM} \cdot \begin{bmatrix} 0 \\ 1 \end{bmatrix} \quad (5)$$

where, u_d and u_q are the phase voltages, i_d and i_q are the phase currents, L_d and L_q are the inductances in direct and quadrature axis respectively. Electromagnetic torque can be obtained by a simple expression of flux linkages and currents as given in equation 6.

$$T_e = \frac{3}{2} \cdot 2p \cdot ((L_d - L_q) \cdot i_d \cdot i_q + \psi_{PM} \cdot i_q) \quad (6)$$

Electromagnetic torque consists of two components. The first term is reluctance torque whereas, the second term represents the synchronous torque. In a PMSM, most of the torque will be generated due to quadrature axis current. Thus, it is fair to assume quadrature-axis current i_q will represent and control the torque output of the machine itself. However, it should be noted that in a highly salient machine as per maximum torque per ampere approach, direct-axis current i_d has to be utilized to generate maximum torque. For most of the applications

that use low saliency machines, i_d is kept zero in operations below nominal speed and torque is generated and measured solely by i_q .

FOC exploits the simple mathematical model of PMSM in $d-q$ axis and utilizes speed and current controllers in $d-q$ coordinate system. A generalized block scheme of FOC is given in Fig. 1. There are 3 PI controllers in this scheme. First PI controller controls the speed and generates i_q reference. Other two PI controllers control the current. Current controllers in synchronous frame outputs voltage references v_d and v_q . These reference values are then transformed into $\alpha-\beta$ coordinate system and applied to stator phases using space vector modulation. Phase currents are then sampled and converted into $d-q$ coordinate system. It can be seen that there are two inner loops for current and one outer loop for speed control in a FOC system. Control frequency for the speed loop is generally determined based on the mechanical inertia of the system. Current control loops are related with time constant of the stator phases and usually a lot frequent than speed control loop.

3. EXTENDED BACK-EMF OBSERVER

Extended back-EMF model of the PMSM in $\alpha-\beta$ coordinate system is obtained from the model in $d-q$ coordinate system. Phase voltage equation given in equation 5 is re-written with a symmetrical inductance matrix as given in equation 7.

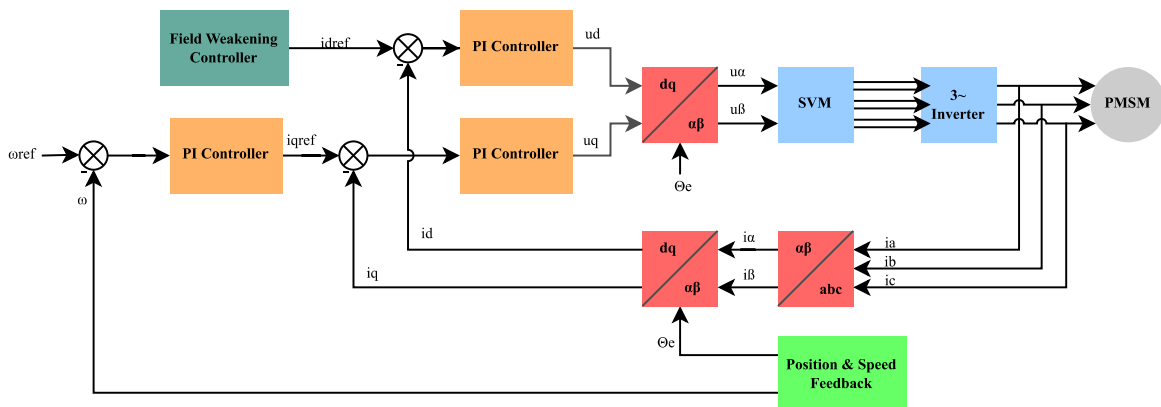


Figure 1 General block diagram of FOC

$$\begin{bmatrix} u_d \\ u_q \end{bmatrix} = \begin{bmatrix} R_s + \rho L_d & -\omega_e L_q \\ \omega_e L_q & R_s + \rho L_d \end{bmatrix} \cdot \begin{bmatrix} i_d \\ i_q \end{bmatrix} + \left((L_d - L_q) \cdot (\omega_e \cdot i_d - \rho i_q) + \omega_e \cdot \psi_{PM} \right) \cdot \begin{bmatrix} 0 \\ 1 \end{bmatrix} \quad (7)$$

Equation 8 is obtained after applying inverse Park transformation.

$$\begin{bmatrix} u_\alpha \\ u_\beta \end{bmatrix} = \begin{bmatrix} R_s + \rho L_d & \omega_e (L_d - L_q) \\ -\omega_e (L_d - L_q) & R_s + \rho L_d \end{bmatrix} \cdot \begin{bmatrix} i_\alpha \\ i_\beta \end{bmatrix} + \left((L_d - L_q) \cdot (\omega_e \cdot i_d - \rho i_q) + \omega_e \cdot \psi_{PM} \right) \cdot \begin{bmatrix} -\sin(\theta_e) \\ \cos(\theta_e) \end{bmatrix} \quad (8)$$

In this expression, rightmost term can be considered as the extended back-EMF part of the model as it contains crucial information of rotor electrical position.

Equation 8 is then re-arranged with back-EMF term is replaced with back-EMF matrix and the model is transformed into Laplace domain as given in equation 9.

$$\begin{bmatrix} u_\alpha \\ u_\beta \end{bmatrix} = \begin{bmatrix} R_s + sL_d & \omega_e (L_d - L_q) \\ -\omega_e (L_d - L_q) & R_s + sL_d \end{bmatrix} \cdot \begin{bmatrix} i_\alpha \\ i_\beta \end{bmatrix} + \begin{bmatrix} e_\alpha \\ e_\beta \end{bmatrix} \quad (9)$$

This relatively easy model to implement estimators and observers will only estimate the extended back-EMF part of the model. Using of a Luenberger observer is very typical for such application that requires state estimation with a feedback observer. In order to obtain rotor position information, two current observers are used in α and β axis. These observers are based on motor model given in equation 9 except the extended back-EMF part is removed from this model. Both observers utilize a compensator that corrects the error between estimated and measured currents. Assuming the observer is stable, current error in steady state will diverge to zero, making the compensators to output the back-EMF part of the model. Compensator outputs $L(\alpha)$ and $L(\beta)$ correspond to $(-e_\alpha)$ and $(-e_\beta)$ respectively.

Control block diagram of the extended back-EMF observer is given in Fig. 2. In this block diagram, estimated state variables are shown as \hat{i}_α , \hat{i}_β , \hat{e}_α and \hat{e}_β . They represent the estimation of α - β axis currents and extended back-EMF terms. The compensator block consists of a simple PI controller.

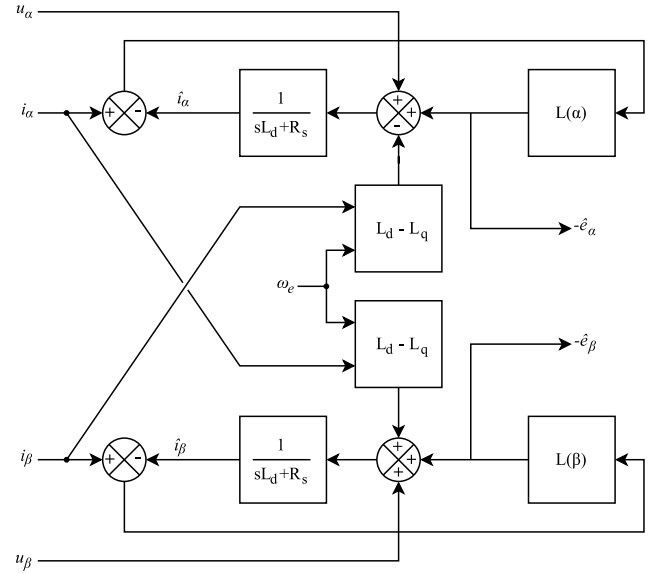


Figure 2 Extended back-EMF observer block diagram

3.1. Angle Tracking Observer

Estimated back-EMF signal obtained from the observer has to be decomposed and rotor position has to be extracted from the back-EMF signals. Many applications utilize an observer for this task. These observers are called as angle-tracking observers. A very simple angle-tracking observer can be implemented using the trigonometric subtraction formula of the sinus signal as given in equation 10.

$$\sin(\theta_e) \cos(\hat{\theta}_e) - \cos(\theta_e) \sin(\hat{\theta}_e) = \sin(\theta_e - \hat{\theta}_e) \quad (10)$$

This equation can be made if α and β components of estimated back-EMF signals are considered as sine and cosine values of θ_e . Right hand side of the equation is the sinus function of error between the position of back-EMF signal and estimated

position obtained from angle-tracking observer’s output. If this error is small, then this equation can be approximated to position error of the observer as given in equation 11.

$$\sin(\theta_e - \hat{\theta}_e) \approx \theta_e - \hat{\theta}_e \tag{11}$$

Angle-tracking observer utilizes an integrator coupled with a PI controller for compensation. PI controller clears position error by outputting the estimated rotor electrical position while the integrator provides a filter to the input signal and improves ramp response. For a more practical approach, integrator and PI controller block places are switched. This provides rotor electrical speed as the output of PI controller and rotor electrical position as the output of the integrator. This arrangement is more convenient as it provides smooth information of speed and position simultaneously. Block diagram of the angle-tracking observer is given in Fig. 3.

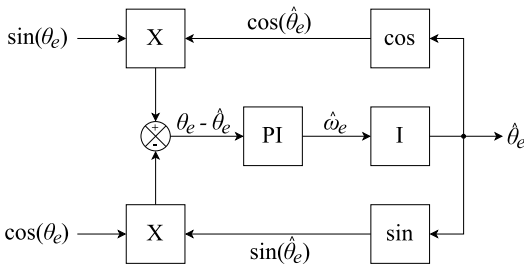


Figure 3 Angle tracking observer block diagram

4. SIMULATION OF THE SENSORLESS DRIVE SYSTEM

In order to verify position estimation schemes, a simulation model is created in MATLAB Simulink (MathWorks, Natick, MA, USA) environment. The motor parameters given in Table 1 are used for the motor model. These motor parameters belong to an actual motor that is used in industrial fan systems, which is then used in experimental work phase of the study. System is modeled and simulated as a continuous system. The simulation starts with no-load and

3000 rpm speed reference. Nominal torque of 0.2 Nm is applied at 0.75 s simulation time. Speed reference is generated by speed ramp generator block. Simulations are done with 6000 rpm/s selected as acceleration and deceleration ratio.

Table 1 Motor parameters

Parameter	Unit	Value
Nominal Voltage	[V]	24
Nominal Current	[A]	3.4
Nominal Power	[W]	62
Nominal Torque	[Nm]	0.2
Peak Torque	[Nm]	0.6
Nominal Speed	[rpm]	3000
Pole Pairs	-	2
Back-EMF Constant	[V.sec/rad]	0.0023
R _s	[Ω]	0.437
L _d	[mH]	0.536
L _q	[mH]	0.548

Speed controller minimizes the error between desired and estimated speed using a PI controller that outputs the i_q reference. Two PI controllers for motor currents are used for compensation that output d - q axis voltage references. They are then transformed into three-phase voltages and applied to the stator phases. Output of the extended back-EMF observer are the back-EMF terms. The angle-tracking observer extracts estimated rotor electrical position and speed. Fig. 4 shows the speed estimation performance. Extended back-EMF observer model is given in Fig. 5.

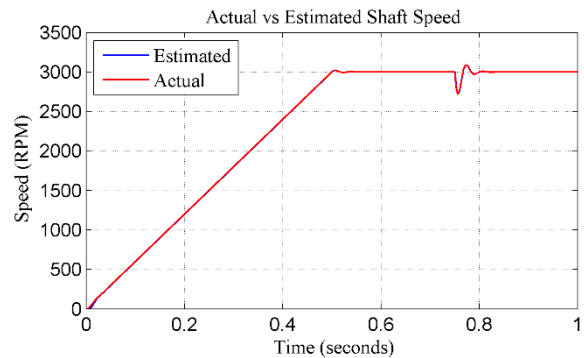


Figure 4 Speed estimation performance

Fig. 6 shows the extended back-EMF estimation with zoomed-in view. Fig. 7 shows the position estimation performance of extended back-EMF observer method.

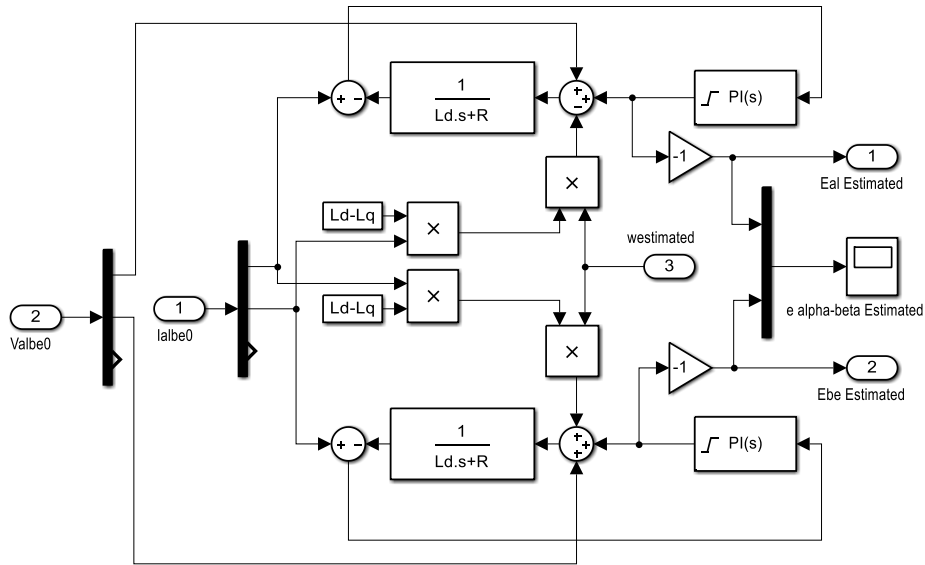


Figure 5 Simulink model of extended back-EMF observer

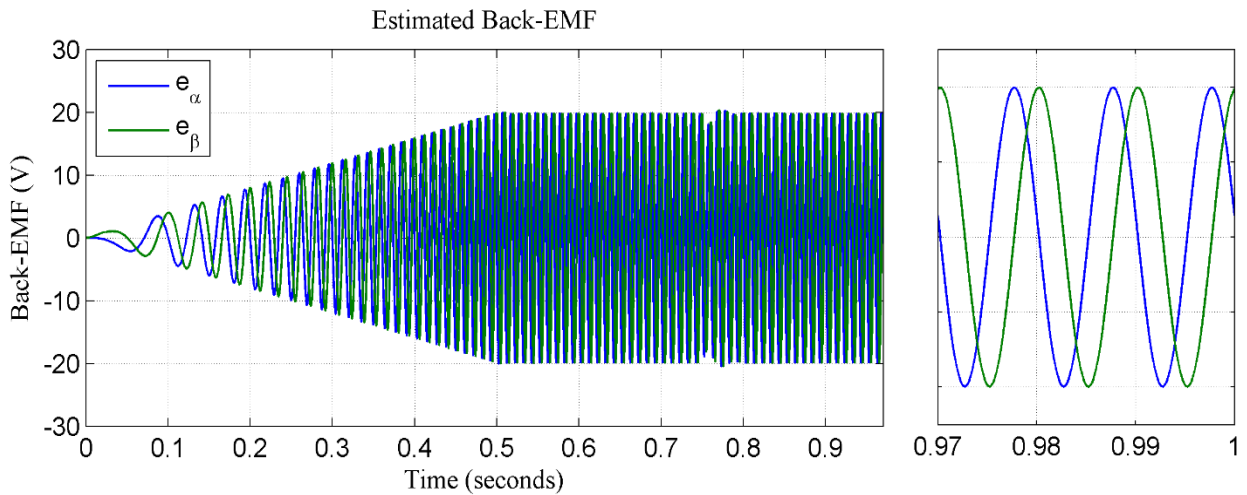


Figure 6 Back-EMF estimation with zoomed-in view

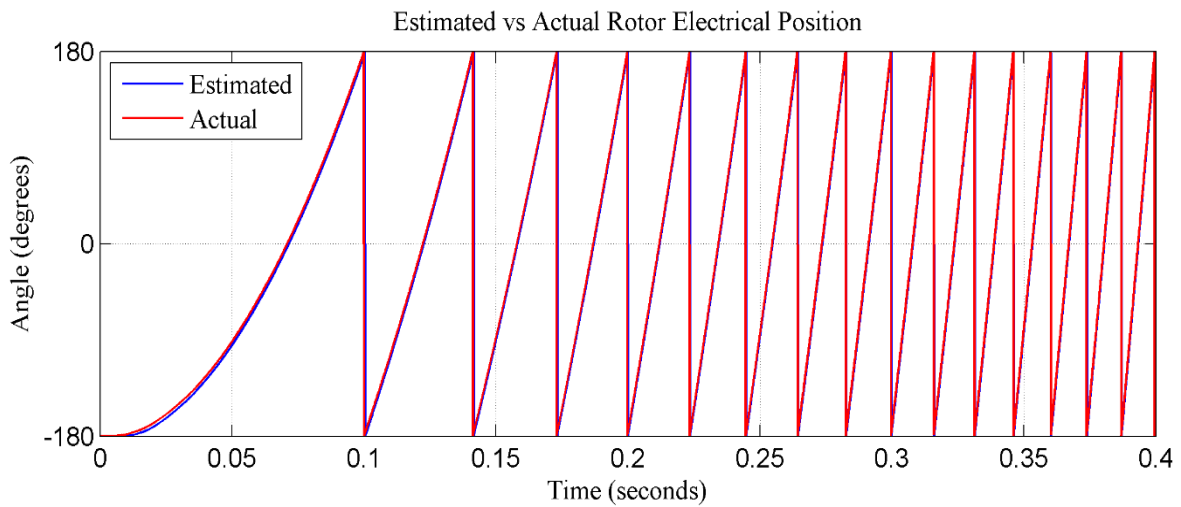


Figure 7 Position estimation performance

It can be said that position estimation is accurate and has a very high dynamic performance. Since the startup is done as open loop, position estimation error from standstill to 200 rpm has no effect on the performance of the control.

Low pass filter used in the angle-tracking observer provides a smooth speed estimation output with no significant delay present. The simulation verifies transient and steady state operation of the extended back-EMF observer with angle-tracking observer.

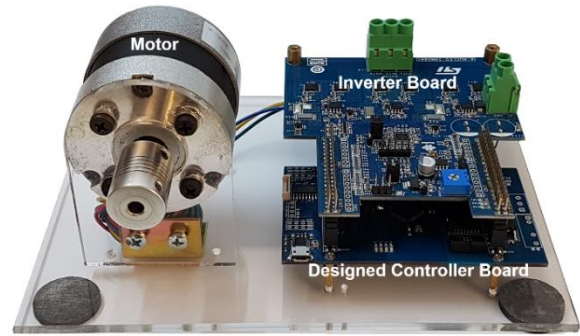


Figure 8 Complete drive system

5. DESIGN OF A SENSORLESS FOC DRIVE

This study concentrates on the design of a controller board and requisite software development for FOC of a PMSM. For the three-phase inverter hardware a ready-to-use development board is selected.

Schematic design of the controller board is made according to the signals that are used in the development board. Two headers are used in order to connect the controller board to the inverter board. Printed circuit board design is done as a two-layer board. Placement of the components is made according to the layout of the inverter board in order to prevent any collisions. Headers are placed according to the headers on the inverter board so that two boards connect easily. Total size of the controller board is 60 x 96.52 mm. Connection of the controller board with the inverter board is done easily as intended. Inverter board has a switching regulator that generates 5V output from the DC supply voltage and this 5V supply is sent to controller board. A linear regulator is used on controller board in order to generate 3.3V logic power supply that provides power for the microcontroller, operational amplifiers and comparators. Fig. 8 shows the designed drive system. DC input power is supplied to the system via a two-contact screw terminal. Three-phase motor output is connected to a three-contact screw terminal.

Embedded software for FOC is developed. The general structure of the software has multiple Finite State Machine (FSM) structures.

Main state machine consists of the states “Init”, “Ready”, “Run” and “Fault” as shown in Fig. 9 along with the state transitions.

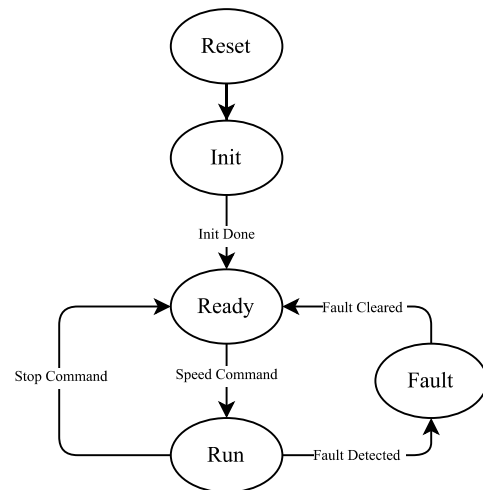


Figure 9 Main state machine diagram

Microcontroller automatically goes through a Power-On Reset (POR) after it is powered up. After the reset microcontroller goes into initialize state. This state defines the functions necessary for initializing requisite microcontroller peripherals such as clock generation, general-purpose timers, pulse width modulation and analog to digital converter. State is automatically changed to ready after initializing is done. When microcontroller is in ready state, speed command is expected as a user input. If a non-zero speed reference is set, then the state transition from ready state to run state is executed.

6. EXPERIMENTAL RESULTS

Experimental verification of the driver system is done by conducted laboratory experiments. The

PMSM with the parameters given in Table 1 is driven with the designed drive system. In order to test dynamic behavior of the system, a test bench that is capable of loading the motor is set up. The test bench consists of a 400V rated PMSM coupled to the driven motor's shaft, which acts as a generator. Output of the generator is rectified using a three-phase rectifier. Obtained DC voltage is then fed into a variable resistor. Setup used for obtaining experimental results is given in Fig. 10.



Figure 10 Experimental test setup

Real time control and data acquisition of the drive system is done using a debugging tool. This tool is capable of sampling and modifying software variables along with a recorder functionality that provide time plots of the signals. Performance of the extended back-EMF observer can be obtained from these graphs. The detailed waveforms of the position estimation scheme in nominal speed are given in Fig. 11.

Performance of the drive system is evaluated by two different tests. No load performance of the system is tested first.

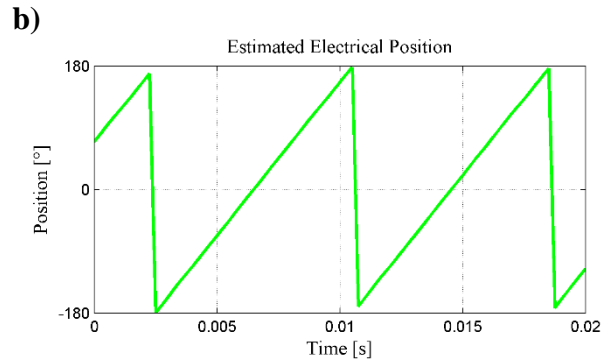
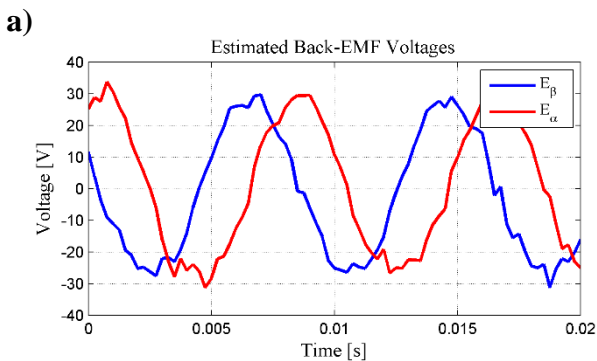


Figure 11 (a) Estimated back-EMF voltages, (b) Estimated electrical position

Applying of nominal speed command with transient changes and speed reversal is tested. Fig. 12 shows the speed ramp and actual shaft speed. Acceleration is set to 2000 rpm/sec. It can be seen that the drive system is capable of following the speed ramp accurately.

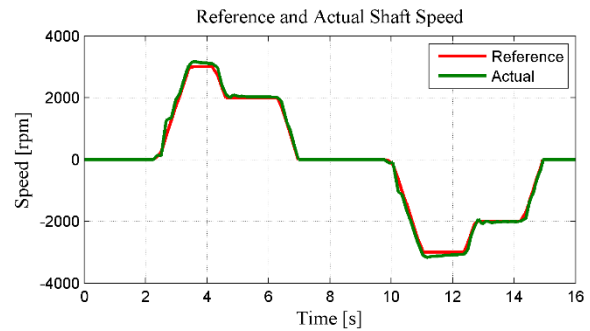


Figure 12 No-load speed control performance

Fig. 13 shows the applied voltages of alpha and beta.

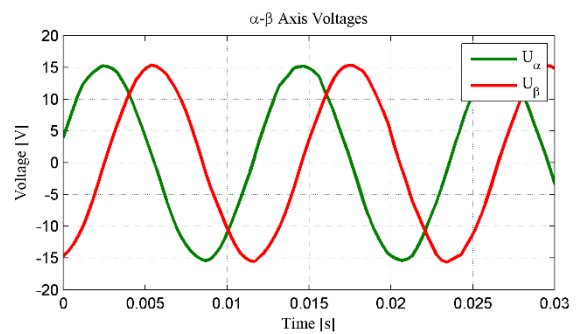


Figure 13 Applied stator voltages in α - β axis

Duty cycles at the output of the space vector modulation corresponding to reference voltages are given in Fig. 14.

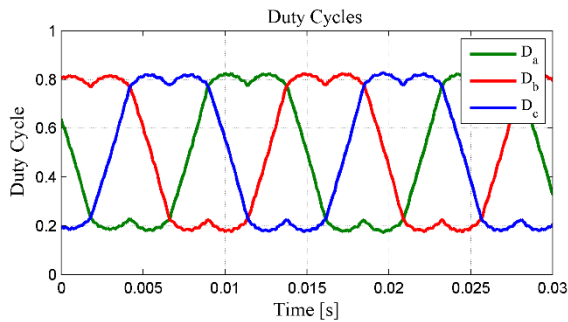


Figure 14 Three-phase duty cycle values

Waveforms of phase currents are shown in Fig. 15.

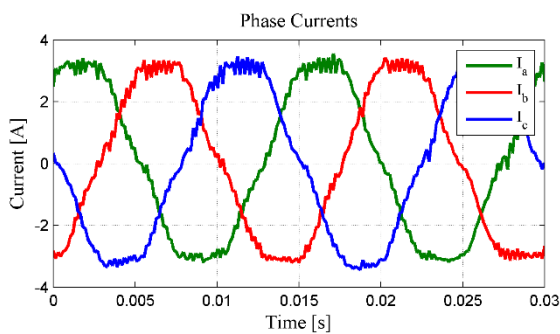
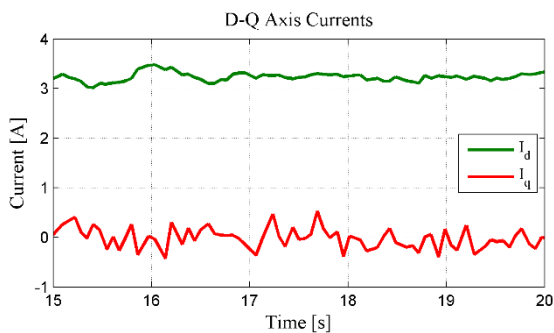


Figure 15 Three-phase currents

Fig. 16 shows the calculated d - q axis currents. It can be seen that the i_d is kept at zero while i_q is increased to nominal load current.

Figure 16 Phase currents in d - q axis

The second test for the validation of the drive system performance was the dynamic response of the system under transient changes on load. This transient load change is achieved by switching the variable resistor to a fixed point. Fig. 17 shows the system variables under transient changes. This graph starts with the machine loaded nominally, then when the time stamp shows 8s, connection to the load resistor is switched off. This sudden load

change causes an overshoot of 10%. Speed overshoot is compensated within approximately 1 second. At time stamp of around 9.5s machine is again fully loaded. This transient loading cause machine shaft speed to decrease about 10%, which is then compensated in approximately 1 second. It is observed that the system remains stable under transient changes in load.

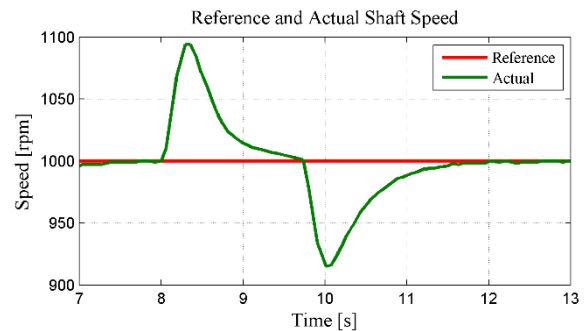


Figure 17 Dynamic performance of the system

7. CONCLUSION

In this study, an industrial-grade sensorless FOC drive system for PMSM using extended back-EMF observer is designed and implemented. Scope of this study covers design of the control stage along with the embedded software. For the sensorless position estimation extended back-EMF observer is analyzed in detail. This observer is a Luenberger type state observer that utilizes the system model inside the controller. State estimation is based on processing measured and known state variables into the system model. Verification of the sensorless position estimation is done using simulations. This is achieved by creating a FOC drive model simulation for extended back-EMF observer. Position estimation is compared with actual position and it is found out that estimation is accurate and dynamic. Sensorless drive system is also implemented in hardware and software. System verification is done by conducting laboratory experiments; 24 V, 62 W, 3000 rpm motor that is been used in industrial fan applications is driven. No-load and full-load performance of the system is tested along with the transient loadings. Transient and steady state response of the system is found stable and dynamic. Along with the successful results of the experiments, an industrial-grade drive system that is re-configurable and flexible is obtained.

Such a system is capable of replacing existing conservative solutions and thus offer greater customization.

Funding

The author (s) has no received any financial support for the research, authorship or publication of this study.

The Declaration of Conflict of Interest/ Common Interest

No conflict of interest or common interest has been declared by the authors.

Authors' Contribution

The first author contributed 60%, the second author contributed 40% to the study.

The Declaration of Ethics Committee Approval

This study does not require ethics committee permission or any special permission.

The Declaration of Research and Publication Ethics

The authors of the paper declare that they comply with the scientific, ethical and quotation rules of SAUJS in all processes of the paper and that they do not make any falsification on the data collected. In addition, they declare that Sakarya University Journal of Science and its editorial board have no responsibility for any ethical violations that may be encountered, and that this study has not been evaluated in any academic publication environment other than Sakarya University Journal of Science.

REFERENCES

- [1] D. Maheswaran, V. Rangaraj, K. K. J. Kailas and W. A. Kumar, "Energy efficiency in electrical systems," 2012 IEEE International Conference on Power Electronics, Drives and Energy Systems (PEDES), pp. 1-6, 2012.
- [2] Directive 2009/125/EC of the European Parliament and of the Council of 21 October 2009 establishing a framework for the setting of ecodesign requirements for energy-related products, OJ L 285, pp. 10–35, 2009.
- [3] T. Ohtani, N. Takada and K. Tanaka, "Vector control of induction motor without shaft encoder," IEEE Transactions on Industry Applications, vol. 28, no. 1, pp. 157-164, 1992.
- [4] C. Schauder, "Adaptive speed identification for vector control of induction motors without rotational transducers," IEEE Transactions on Industry Applications, vol. 28, no. 5, pp. 1054-1061, 1992.
- [5] L. Li, X. Guo, P. Zeng, Z. Li, K. Chen and J. Cao, "Sensorless Vector Control for Automotive Auxiliary Motors in the Full Speed Range," 2019 22nd International Conference on Electrical Machines and Systems (ICEMS), pp. 1-4, 2019.
- [6] S. Padhy, R. M. Pindoriya, C. Subramanian and Z. Husain, "Encoder-less speed control of PMSM drive using adaptive observer," 2018 IEEMA Engineer Infinite Conference (eTechNxT), pp. 1-6, 2018.
- [7] V. Medam, S. Basak, Y. T. Rao and C. Chakraborty, "An adaptive rotor resistance estimation technique for vector controlled induction motor drive suitable for electric vehicle application," IECON 2019 - 45th Annual Conference of the IEEE Industrial Electronics Society, pp. 2604-2609, 2019.
- [8] J. Holtz and Juntao Quan, "Sensorless vector control of induction motors at very low speed using a nonlinear inverter model and parameter identification," IEEE Transactions on Industry Applications, vol. 38, no. 4, pp. 1087-1095, 2002.
- [9] L. Yan and X. Song, "Design and Implementation of Luenberger Model-Based Predictive Torque Control of Induction Machine for Robustness Improvement," IEEE Transactions on Power Electronics, vol. 35, no. 3, pp. 2257-2262, 2020.

- [10] T. Orłowska-Kowalska, "Application of extended Luenberger observer for flux and rotor time-constant estimation in induction motor drives," *IEE Proceedings D - Control Theory and Applications*, vol. 136, no. 6, pp. 324-330, 1989.
- [11] J. Lai, C. Zhou, J. Su, M. Xie, J. Liu and T. Xie, "A Permanent Magnet Flux Linkage Estimation Method Based on Luenberger Observer for Permanent Magnet Synchronous Motor," 2019 22nd International Conference on Electrical Machines and Systems (ICEMS), pp. 1-6, 2019.
- [12] F. P. Scalcon, C. J. Volpato, T. Lazzari, T. S. Gabbi, R. P. Vieira and H. A. Gründling, "Sensorless Control of a SynRM Drive Based on a Luenberger Observer with an Extended EMF Model," *IECON 2019 - 45th Annual Conference of the IEEE Industrial Electronics Society*, pp. 1333-1338, 2019.
- [13] M. F. Moussa, Y. Gaber and M. El Attar, "Vector control drive of permanent magnet motor without a shaft encoder," 2008 12th International Middle-East Power System Conference, pp. 249-254, 2008.
- [14] G. Chen, S. Yang and J. Chen, "Advantages of Flux-based Position Sensorless Drive for Surface Permanent Magnet Machine," *IECON 2019 - 45th Annual Conference of the IEEE Industrial Electronics Society*, pp. 899-903, 2019.
- [15] G. Chen, J. Chen and S. Yang, "Implementation Issues of Flux Linkage Estimation on Permanent Magnet Machine Position Sensorless Drive at Low Speed," *IEEE Access*, vol. 7, pp. 164641-164649, 2019.
- [16] G. Garcia Soto, E. Mendes and A. Razek, "Reduced-order observers for rotor flux, rotor resistance and speed estimation for vector controlled induction motor drives using the extended Kalman filter technique," *IEE Proceedings - Electric Power Applications*, vol. 146, no. 3, pp. 282-288, 1999.
- [17] M. S. Termizi, J. M. Lazi, Z. Ibrahim, M. H. N. Talib, M. J. A. Aziz and S. M. Ayob, "Sensorless PMSM drives using Extended Kalman Filter (EKF)," 2017 IEEE Conference on Energy Conversion (CENCON), Kuala Lumpur, pp. 145-150, 2017.
- [18] V. I. Utkin, "Sliding mode control design principles and applications to electric drives," in *IEEE Transactions on Industrial Electronics*, vol. 40, no. 1, pp. 23-36, Feb. 1993.
- [19] J. Sun, G. Cao, S. Huang and Q. Qian, "A Sliding Mode Observer for Position Estimation of the Planar Switched Reluctance Motor," 2019 IEEE International Electric Machines & Drives Conference (IEMDC), San Diego, CA, USA, pp. 1342-1347, 2019.